



Model processes and cavitation indicators for a quantitative description of an ultrasonic cleaning vessel: Part I: Experimental results

Matthias Jüschke*, Christian Koch

Physikalisch-Technische Bundesanstalt, Bundesallee 100, 38116 Braunschweig, Germany

ARTICLE INFO

Article history:

Received 10 June 2011

Received in revised form 20 December 2011

Accepted 24 December 2011

Available online 3 January 2012

Keywords:

Cavitation

Sonoluminescence

Sonochemistry

Erosion

ABSTRACT

In this paper, four sensor types are presented for quantitative measurements in an ultrasonic cleaning vessel: (1) a hydrophone to measure spectral components of the sound field; (2) an aluminium foil technique as a model process for erosion; (3) a test tube filled with a solution of luminol to measure the emission of light; and (4) a test tube filled with potassium iodide solution to measure the oxidation of iodide. Thus a broad range of diverse cavitation effects is covered. The quantities were measured in dependence on three parameters: the electrical input power of the transducers, the temperature and the O₂ concentration of the water. To ensure constant environmental conditions, a flow system was built up which continuously exchanges the water in the vessel. The comparability of the data measured in subsequent measurement cycles is discussed and the influence of the different sensor types on the cavitation field is considered. Dependences on the three parameters are shown. A quantitative analysis of correlations between the data is carried out in the second part of the study (Koch and Jüschke, 2012 [1]).

© 2012 Elsevier B.V. All rights reserved.

1. Introduction

Cavitation is applied in many areas of technical [2,3] and medical processing or treatment [4]. Describing and understanding the phenomena is a key element of specific and effective application in different fields. A significant number of studies and works have been carried out for the investigation of single bubble dynamics as a representative model of cavitation [5–7]. Important properties such as bubble oscillation, resonance frequency, cavitation threshold, or temperature and pressure in the bubble were derived, and conclusions were drawn on the effect of bubble activity. Since the interaction between bubbles dramatically changes the behaviour of the bubbles, the conclusions from single-bubble to application effects are limited.

Bubble–bubble interaction causes several features specific to the behaviour of bubble clouds, mainly the formation of macroscopic structures with a typical visual appearance due to Bjerknes forces between the bubbles [8,6]. These structures change the effect of cavitation, for example in cleaning applications [9]. Since the number of bubbles in a cavitation cloud reaches several million, the complete mathematical solution of the many-particle problem is not possible, although models with generalised parameters yield interesting results [7,10,11] and can simulate typical bubble traces [12] in structures. The influence of bubble clusters on practical cavitation effects, for example during cleaning or sonochemistry, is, however, not yet well understood.

A common way to overcome problems with models on a microscopic scale is the determination of experimentally available macroscopic measurands which are closely connected to effects of cavitation [13]. A typical example is the treatment of an aluminium foil in an ultrasonic vessel [14,15] which is used as a model representing the erosion effect of cavitation. Because of its simple handling, it is widely used especially in testing practice at the manufacturers' of ultrasonic vessels, although the relation, for example, to the cleaning effect is not clearly supported [16–18]. The measurement of the sound field is quite attractive for the process description because the sound field is the driving force of acoustic cavitation. A cavitation intensity was deduced from the acoustic emission spectrum [19], but there not always clear relations to further cavitation effects [20,21]. The subharmonic, for example, often identified as a cavitation indicator, cannot be clearly correlated to chemical or erosion effects [16,20,22,23]. In another study, the maximum bubble radius was theoretically deduced from sound field measurements and a correlation to chemical output was found [24]. As an alternative to describe chemical effects, luminescence was observed considering the vessel as a whole [25]. Recently, the sound pressure components and luminescence as a function of the distance from the transducer were evaluated [26]. Also, biological effects correlate with different sound fields or other experimental values in different cases of application [27,28].

It seems that there is no single indicator that could describe a wider spectrum of cavitation applications. This study focuses on the quantitative evaluation of cavitation activity in a bath using different sensor techniques and a multivariate data analysis. It

* Corresponding author. Tel.: +49 531 592 1461; fax: +49 531 592 1605.

E-mail address: matthias.jueschke@ptb.de (M. Jüschke).

compares very different outcomes of cavitation under carefully controlled environmental conditions in a wider parameter range as in studies before. The experimental results are presented in part I of the paper. In the second part, the data were used for a multivariate data analysis which is a quite novel strategy for cavitation analysis [1].

In this work, a set of four model processes is applied to an ultrasonic vessel which covers a wide range of cavitation effects. Sound field measurement, an erosion indicator, a chemical indicator and sonochemical luminescence, which are all determined at confined local positions, are combined to form a set of indicators for describing the cavitation field in the cleaning vessel. All indicators and parameters are set in relation to each other, and correlations, dependences and overlappings are investigated. This is realised in particular with a structure-finding statistical method as part of a multivariate data analysis. A factor analysis is applied which is first used to find relations and overlappings between all variables by finding common factors. In a second step, a method is developed for a general strategy of a description of cavitation processes by a reduced set of measurands.

The two parts of this study are organised as follows. This paper first describes the experimental set-up and the methods for the determination of indicators. Then, results for the determined indicators are presented and relations between them and their dependence on experimental parameters such as temperature or O_2 concentration of water are investigated and discussed. The second part focuses on the application of factor analysis. After a brief introduction into the background of this method, results for different cases of application are presented which give insight into deeper relations between indicators and parameters. From the fundamentals of factor analysis, a method is developed for a general strategy for the quantitative description of cavitation processes in a wide range of applications.

2. Experimental set-up

2.1. Vessel set-up

For the experiments, a commercial cleaning vessel (TI-H-5, Elma GmbH & Co., KG, Singen, Germany) with a base area of $130 \times 240 \text{ mm}^2$ was used. It was filled to a level of 115 mm (about 3.6 litres) with deionised water. Fig. 1 shows a sketch of the experimental set-up. For constant environment conditions, the water was continuously changed under laminar flow conditions with a

flux of about 1.8 litres/min and pumped back to a reservoir of 80 litres at the maximum filling height. In this way, changes in temperature and gas concentration of the water were minimised during the measurement phase. The surface of the water in the vessel was covered with a plastic foil to reduce water surface movement.

In this study, the operating frequency f_0 of the vessel was kept constant and a synthesizer (3326A, Hewlett–Packard Company, Palo Alto, USA) was used as a signal source at $f_0 = 44.3 \text{ kHz}$. The voltage amplitude of the synthesizer U_S was controlled by a computer and set to $U_S = 3.5 \text{ V}$ at maximum. The synthesizer output was fed into an audio-amplifier (the t.amp Proline 1800, Musikhaus Thomann e.K., Burgebrach, Germany) and the amplifier output was connected to an impedance matching network driving two ultrasound transducers which were mounted at the bottom of the vessel.

To determine the effective electrical input power, the voltage and the current of the driving signal were measured. The current was determined using a current probe with amplifier (P6021 with amplifier type 134, Tektronix Inc., Beaverton, USA) connected to an oscilloscope (DPO 3012, Tektronix Inc., USA) which also detected the voltage. The effective power was calculated by multiplying and averaging the corresponding values of voltage and current. The temperature (using a 4-wired PT100 element) and the O_2 concentration (HQ 30d, Hach-Lange GmbH, Düsseldorf, Germany) – as an indicator for the solved gas concentration – of the water in the vessel were measured at the outlet flow.

In different measurement cycles, the parameters electrical power, temperature and O_2 concentration were varied. The electrical input power was changed by controlling the output voltage of the synthesizer U_S . For a measurement cycle in which the temperature was changed, the reservoir was cooled down first. While continuously running measurements, the water then was slowly heated up over several hours. The variation of the O_2 concentration was realised by filling the reservoir with degassed water at the beginning of the experiment. While continuously running measurements, air diffused through the water surface into the volume and the O_2 concentration of the water increased slowly. Each measurement cycle with changing O_2 concentration took several hours and changes during obtaining one measurement point could be neglected. The O_2 concentration was measured with an accuracy of 0.2 mg/L.

Measurements were made at the seven positions indicated in Fig. 1: in the centre of the vessel at a height of 20 mm, 60 mm and 100 mm above the vessel floor and, to get higher sound pressure, in front of one transducer at a height of 41 mm, 46 mm,

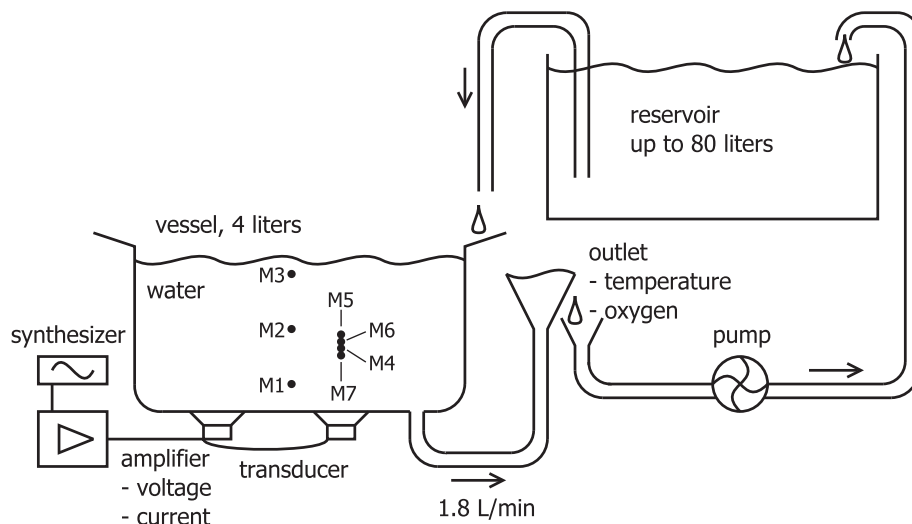


Fig. 1. Experimental set-up with electrical excitation, circular flow of the water and seven measurement positions M1–M7 in the vessel.

51 mm and 56 mm. The positions were chosen in a way that it would have been possible to record different parts of a standing wave, if it had occurred. These measurement positions were defined as M1 to M7, as shown in Fig. 1. Most of the measurements were made at position M4.

Four different sensors - i.e. model processes - were used to quantify cavitation indicators: A hydrophone, an aluminium foil, a luminescence probe and a sonochemistry probe which are presented in the following sections.

2.2. Sound pressure and spectral components

The sound pressure p was measured with a hydrophone (TC4013, Reson A/S, Slangerup, Denmark). The output voltage was acquired using an oscilloscope (TDS 3032B, Tektronix, USA) with a sampling frequency of 5 MHz, and the sound pressure was calculated using the hydrophone sensitivity value at the working frequency f_0 . Sensitivity deviations of the further observed discrete frequencies are in a range of ± 1.5 dB.

Six values of the hydrophone signal were extracted as indicators for cavitation effects. From the time-dependent data the rms pressure value was calculated. To obtain the other five values, the time-dependent waveform was multiplied with a flat top window and the spectrum was evaluated. From the spectral data, the amplitudes of the fundamental at $f_0 = 44.3$ kHz, of the subharmonic at $f_0/2$, of the ultraharmonic at $3/2 f_0$ and of the 2nd harmonic at $2f_0$ were calculated. The cavitation noise was determined in the frequency range from 100 to 200 kHz, leaving out multiples of the subharmonic ($n/2$) f_0 in a range of ± 2.5 kHz around the respective centre frequencies. The cavitation noise is defined as the rms value of the remaining spectral components. All indicators were obtained as the average of eight independent measurements.

2.3. Aluminium foil erosion

A quantitative value for the erosion effect of cavitation was obtained by determining the deformation and destruction of an aluminium foil (Korff AG, Oberbipp, Switzerland). The foil consisted of aluminium alloy 1200 (EN 573–3/4) with a thickness of $15 \mu\text{m}$ and a size of $130 \times 180 \text{ mm}^2$ to fit in a mounting which could be brought into the vessel. The foil cuts were mounted to span the depth and the height of the vessel from 10 mm above the ground up to the surface.

The foil was exposed to the sound field for 20 s. Then an RGB image was taken using a flat bed scanner with a resolution of 300 dpi. Three types of damage were detected: rather smooth dents, burrs and holes [29]: The foils were imaged using a red background. Pixels belonging to holes in the foil were detected by evaluating the fraction of red of a pixel. If the red fraction of a pixel exceeded a certain limit, the pixel was counted as belonging to a hole. The other two erosion components were calculated with the grey-scaled image. For the detection of the burrs, the nearest neighbours of the pixels were considered. If the difference in intensity exceeded a limit, the pixel was counted as a burr. The dents form the most sensitive and most noisy erosion indicator. Structures and not single pixels were taken into account. First, the background of the image was subtracted using a moving median of 21×21 pixels. Then a histogram of grey values was determined. Pixels which lie in a pre-defined grey value range of the histogram were identified as dents.

The counts of the three erosion effects were normalised by the number of pixels in the analysed area, and a relative value c_{er} of the three erosion components was obtained. To get a single erosion value E , the values of dents, burrs and holes are weighted with factors. To estimate these factors, it is assumed that a cavitation

event generates a dent in the foil at first. Further cavitation events shape the foil further and form a burr and finally result in a hole. Thus, holes were values that should have the largest weighting factor; burrs were accounted by a medium factor and dents by the smallest one. The estimation $E = 5 c_{\text{er}}(\text{holes}) + 3 c_{\text{er}}(\text{burrs}) + c_{\text{er}}(\text{dents})$ turned out to be appropriate in comparison with experimental results [1,29]. The values obtained were summed up on an analysed area of 10 mm in lateral dimension and 5 mm in height to be comparable to the hydrophone's outer dimensions.

2.4. Luminescence

For the detection of luminescence a defined solution of luminol was used. 10 mg luminol were solved in 500 ml NaOH base with a pH-value between 10 and 11. To carry out measurements with spatial resolution, this solution was filled in a polyethylene test tube, which has an inner diameter of 12 mm, a length of 30 mm, and a wall thickness of 1 mm (Carl Roth GmbH+Co., KG, Karlsruhe, Germany). The test tube was mounted horizontally with the centre at the measurement positions.

An EMCCD camera (iXon 885, Andor Technology, Belfast, Northern Ireland) was used to take images of the test tubes with constant amplification factors and with 14 bit brightness resolution for each pixel. The spatial resolution was 1004×1002 pixels which were reduced to 502×501 pixels by 2×2 binning to improve the signal-to-noise ratio. The camera was mounted at a distance of about 30 cm above the bottom of the cleaning vessel and the exposure time was 15 s. To remove the dark signal and background noise, the 1st percentile of the light intensity count distribution was subtracted from the intensity values of all image points. The area of the test tube in the image was identified from a reference image obtained during daylight illumination. The median of the light intensity counts in this area comprised the luminescence indicator.

Unfortunately, the water surrounding the test tube in the filled vessel (without luminol) also generated some luminescence. When light occurred between the tube and the camera it could not be distinguished from the luminescence of the tube. However, the effect seemed to remain marginal since it was unlikely that light was produced exactly between the camera and the test tube, and it was less bright (factor of about 3 smaller than the light of the test tube).

2.5. Sonochemistry

For modelling sonochemical effects the Weissler reaction was applied [30]. A potassium iodide solution was sonicated and iodine (I_2) was produced. A fraction of the iodine combines with iodide to form triiodide I_3^- . The triiodide absorbs light with a maximum extinction at 352 nm, and a quantitative determination of the iodine release could be carried out with a spectrometer.

A solution of 0.5 M potassium iodide was prepared. To obtain spatial resolution, the solution was filled in the same kind of tubes as was taken for the luminescence. The tubes were exposed to the ultrasound for 4 min. During this period, the triiodide was generated and the concentration of triiodide in the solution was measured afterwards with a UV/VIS spectrometer (spectroFlex 6600 with quartz cells, WTW GmbH, Weilheim, Germany), detecting the extinction coefficients for wavelengths from 340 to 360 nm. In this range a polynomial of 2nd order was fitted to the extinction values, and the maximum of the fitting curve was taken as the extinction coefficient. If the curve was too noisy or the extinction was too low for the fitting procedure to find the maximum in the considered range, the maximum value of the experimental data was taken.

Table 1
Variances of different indicators.

Indicator	Variance (%)
Rms sound pressure	10
Subharmonic	25
Erosion of Al-Foil	30
Luminescence	20
Weissler reaction	35

2.6. Reproducibility

The reproducibility of the measurements with the different sensors was evaluated for a vessel with gas saturated water at a temperature of 21 °C with driving voltage in the range of 2.5 to 3.0 V. The variances are shown in Table 1 and they are estimated from at least six subsequent measurements.

Variances specific to every measurement cycle are an integral part of the multivariate data analysis described and discussed in the accompanying paper.

3. Results

3.1. Hydrophone measurements

In a first step, the spectral components of the sound field were measured to get an overview of the behaviour of the cavitation in the vessel.

Fig. 2 shows the dependence of the spectral sound field components on the synthesizer voltage U_S , the parameter used to control the electrical power. The measurements are obtained at position M4 (see Fig. 1).

The fundamental and the rms pressure increase monotonically with increasing U_S . For nearly all measurement points and amplitudes, about 80% of the signal power is concentrated in the fundamental. So, taking the factor of $\sqrt{2}$ between the amplitude of a sine wave and its rms value into account, the fundamental and the rms pressure differ only by a power-independent factor of 1.2 to 1.4.

The other indicators show a threshold behaviour at about $U_S = 2.2$ V. The amplitudes of the subharmonic and the ultraharmonic show quite similar power dependence and the second harmonic also has a threshold. For further investigations in this paper, mainly the subharmonic is used as a cavitation indicator. The full spectrum of acoustic indicators is investigated in the second part of this study [1].

3.2. Hysteresis

Next, the influence of the direction of changing the driving voltage amplitude U_S was investigated. First, U_S was increased and when U_S exceeded 2.2 V, the spectral components suddenly changed. By decreasing the amplitude U_S , the step back of the spectral components occurs at lower amplitudes, at about $U_S = 1.7$ V. Fig. 3 shows that the spectral components follow a hysteresis loop. The dark curves give the values while increasing U_S , the grey curves while decreasing U_S . Again, subharmonic, ultraharmonic, and noise show very similar dependences on U_S .

In the centre of the hysteresis region around $U_S = 1.9$ V, the behaviour of the vessel depends on the history of the experiment and cannot be controlled exactly by external parameters. This hinders an objective description of the processes by, for example, a functional relation between the external parameters and the cavitation indicators. For an overall description, statistical means can be applied as shown in the second part of this study.

3.3. Comparison of non-simultaneous measurements

The various measurements of the indicators obtained from the hydrophone, the aluminium foil, the luminescence and the sonochemical reaction introduced in Section 2 should be recorded within one measurement cycle. For practical reasons, changing the sensors at each adjusted value of temperature or O_2 concentration, however, was not possible. Therefore, the variations in electrical power, temperature, and O_2 concentration were made subsequently for each sensor.

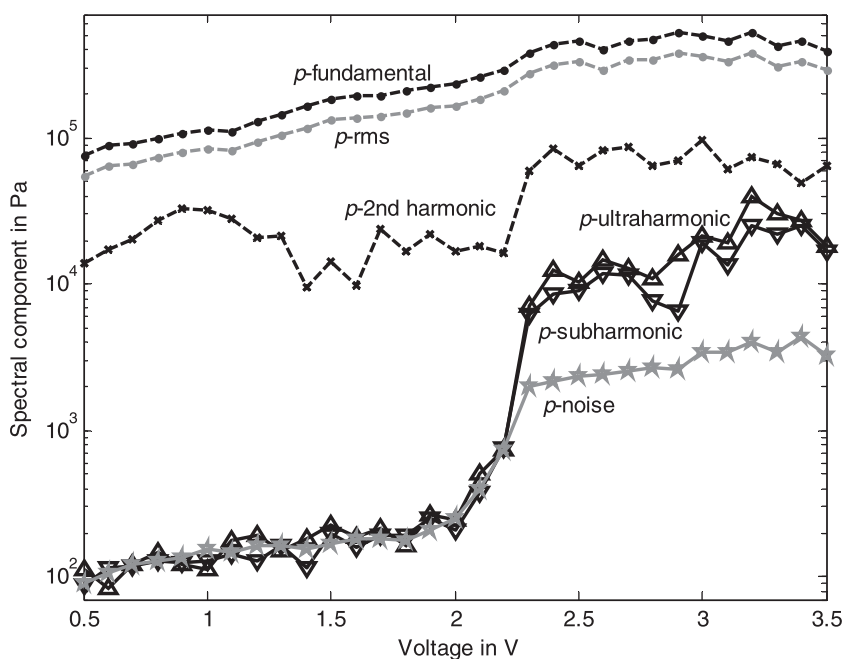


Fig. 2. Sound field components as a function of synthesizer amplitude measured at position M4.

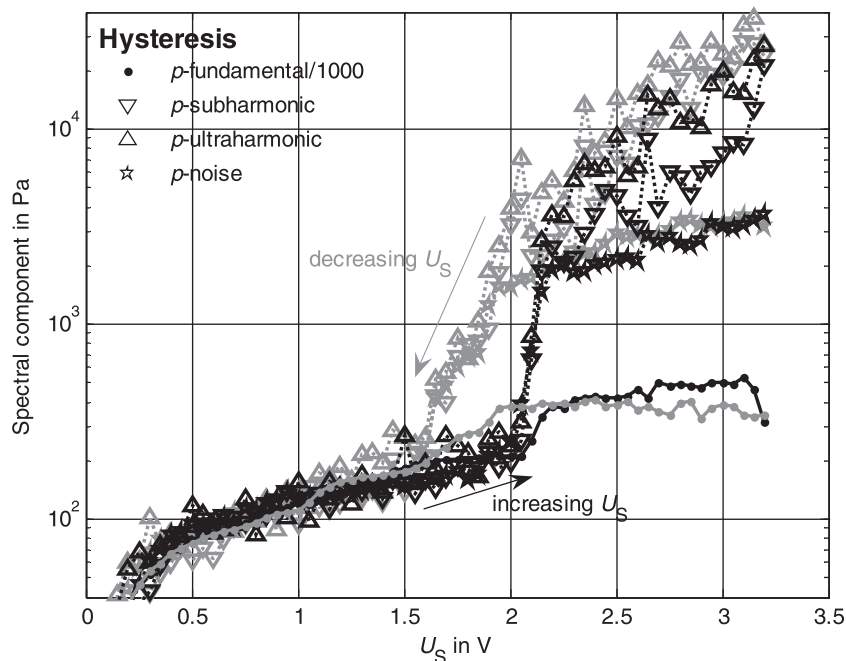


Fig. 3. Hysteresis of spectral components by sweeping U_S at measurement position M4.

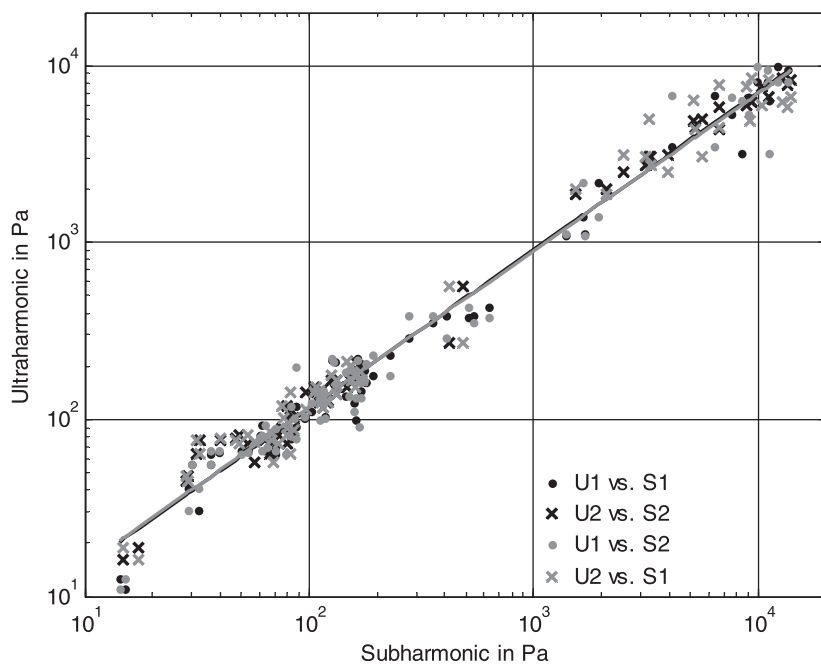


Fig. 4. Relation between the subharmonic (S) and the ultraharmonic (U) compared for measurements from the same cycle (black) and from two subsequent cycles (grey), each for increasing and decreasing U_S .

To estimate if subsequent measurements deliver comparable results, the sub- and the ultraharmonic of two different subsequent measurements are plotted in Fig. 4 while increasing U_S from 0.1 to 3.2 V and decreasing back to 0.1 V. The measurements were performed at the position M4. The black symbols show the ultraharmonic as a function of the subharmonic for values of the same measurements. As seen in the measurements of Fig. 2 and Fig. 3, both indicators produce quite identical behaviour with respect to electrical power as a parameter, and in Fig. 4 they are located along

a straight line which represents a linear fit. Grey symbols show the subharmonic of the first measurement versus the ultraharmonic of the second one, and vice versa. All the straight lines in the figure are linear fits for each of the four comparisons, and plots with simultaneous and with subsequent components are in good agreement. The scattering of the interchanged (grey) values increases slightly only for large amplitudes. The quality of the fit can be estimated from the r^2 -values which are $r^2 = 0.985$ for the same measurements and $r^2 = 0.972$ for the interchanged values. Thus, the

subsequent measurements can be related to each other. We assume this result holds for the other sensors so that the indicators from succeeding measurements can be compared as well.

3.4. Dependence of subharmonic on power and temperature

For some indicators the measurement time is too long to record many data. To judge whether the measurement points may be reduced to single point recordings of the subharmonic at the points M1–M7 are compared.

Fig. 5 shows the subharmonic measured at the seven measurement positions in the vessel and plotted as a function of temperature using the same line markers for four settings of U_S . Varying the temperature, the subharmonic exceeds a threshold at different voltages

U_S . As can be seen in Fig. 5, for increasing voltages the threshold temperature of the subharmonic decreases. For $U_S > 2.5$ V the maximum of the subharmonic is reached near 25 °C; the drop for higher temperatures is analysed in the discussion of Fig. 6. At temperatures below 14 °C, however, the subharmonic increases.

The working frequency f_0 was chosen in advance of the shown experiments at a temperature of 20 °C for the best electrical power input. If the temperature increases, the resonance frequency of the vessel changes due to the lower speed of sound in the water while the filling height remains constant and a temperature dependence of electrical power is observed. Fig. 6 shows the dependence of the electrical power as a function of the temperature with U_S as a parameter. The scattering of the curves plotted with identical markers shows the scattering of the electrical power. For temper-

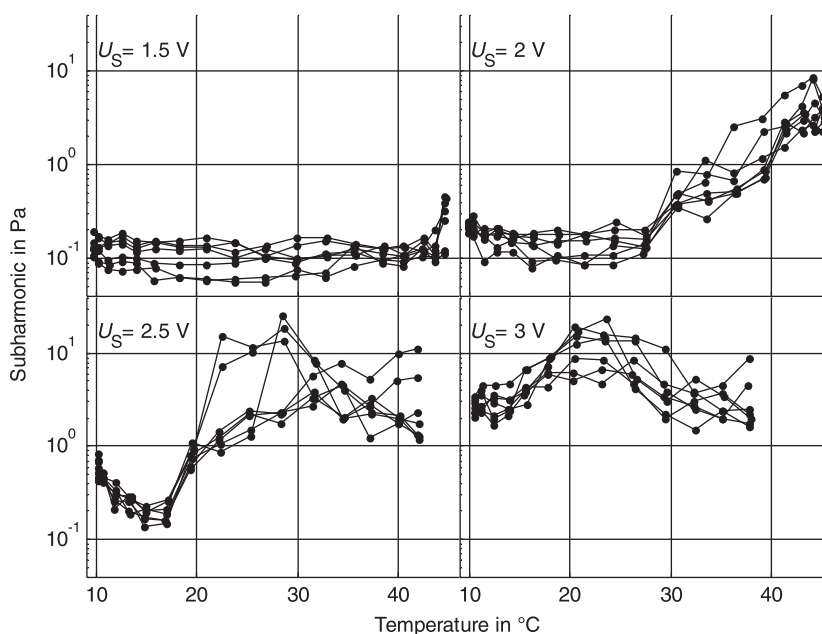


Fig. 5. Dependence of the subharmonic on the temperature, U_S varies in the range from 1.5 to 3 V for the 7 measurement positions shown in Fig. 1.

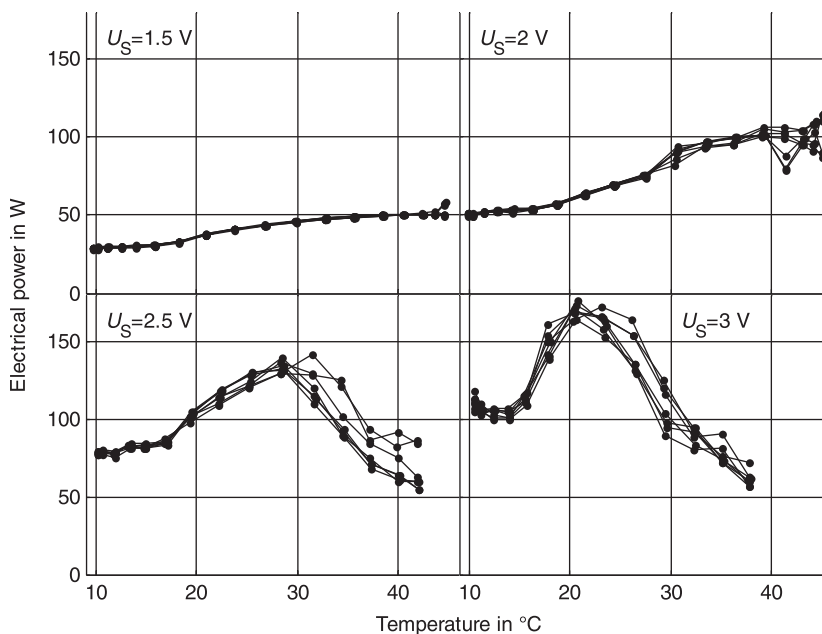


Fig. 6. Dependence of the measured electrical power on the temperature for different amplifier voltages U_S .

atures above 20 °C and $U_S \geq 2.5$ V the corresponding electrical power decreases with increasing temperature although, as can be seen in Fig. 5, the subharmonic remains above the threshold level. Because of the scattering of the electrical power, it was not possible to adjust it to a preset value and it was handled as a measured indicator. Instead, U_S was always used as a parameter for setting the applied input power. The dependence of other indicators on electrical power can be seen in Fig. 7.

3.5. Dependence of various indicators on external parameters: power, temperature and O_2 concentration

As demonstrated for the subharmonic as a function of U_S , threshold behaviour also occurred for the other indicators introduced in Section 2. Fig. 7 shows selected indicators in dependence on the electrical power and normalised to their maximum values. The normalizing factors are given in the legend. The temperature

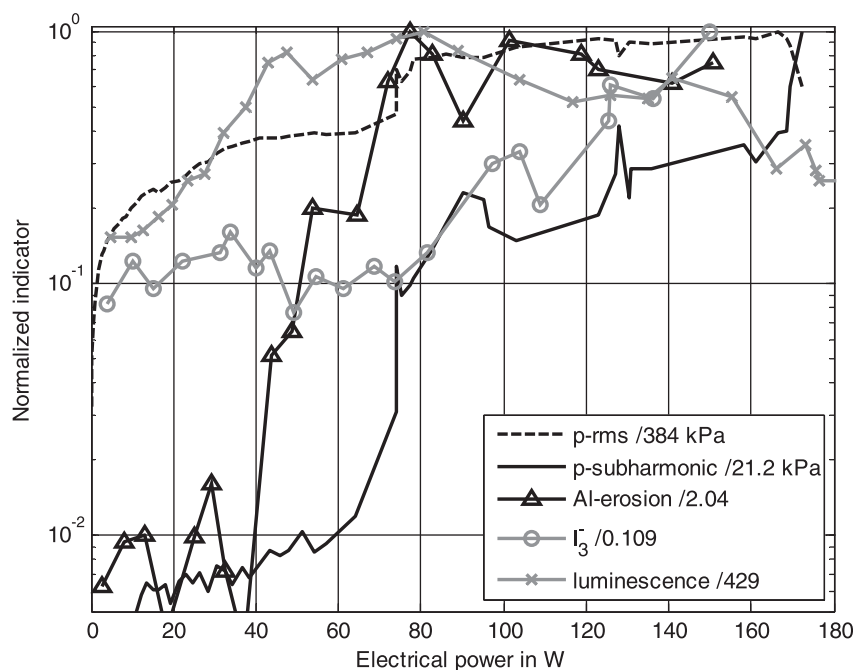


Fig. 7. Dependence of normalised cavitation indicators on the electrical input power of the transducers. Indicators measured at M4. The normalizing factors are given in the legend.

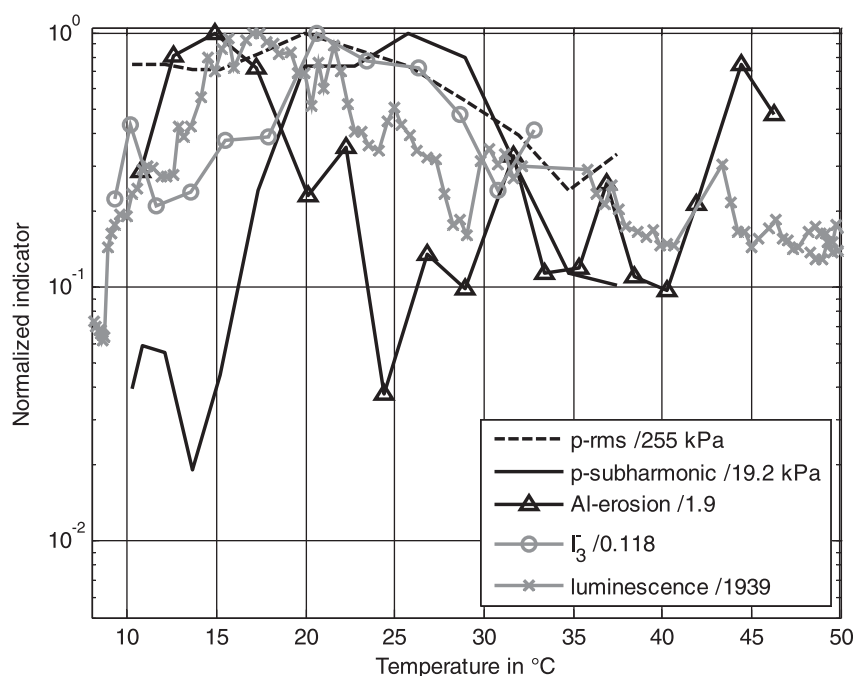


Fig. 8. Dependence of normalised cavitation indicators on the temperature for $U_S = 2.75$ V. Indicators measured at position M4. The normalizing factors are given in the legend.

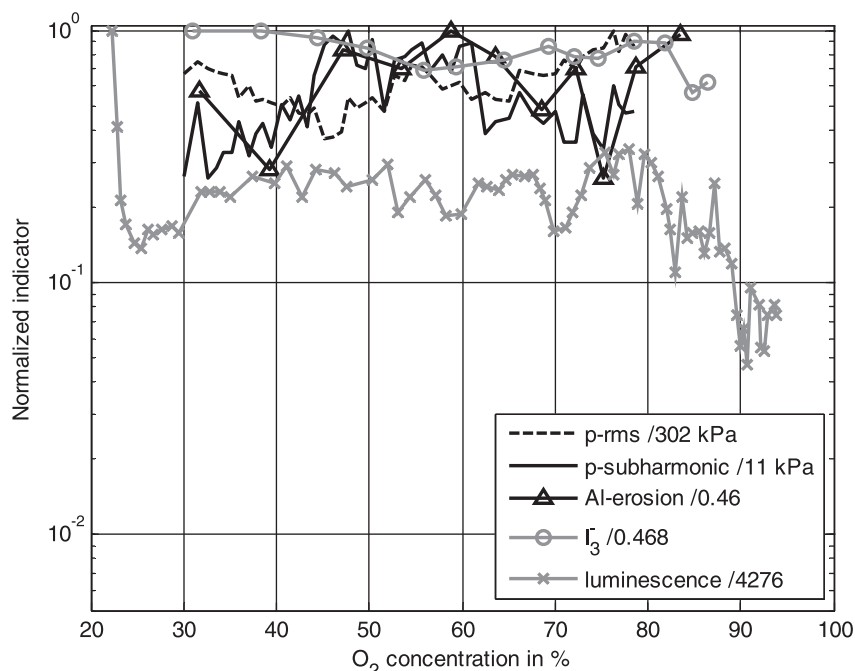


Fig. 9. Dependence of normalised cavitation indicators on the O_2 concentration for $U_S = 2.75$ V at 20 °C. Indicators measured at position M4. The normalizing factors are given in the legend.

was set to 21 °C and the O_2 concentration was kept at 100% . All indicators were measured at position M4.

The electrical power values where the indicators exceed a threshold level differ. The luminescence has the lowest threshold at about 30 W. The luminescence decreases above 80 W. Such behaviour at high power is in agreement with other studies [25,31,32]. The threshold for the aluminium foil erosion indicator amounts to 45 W. The subharmonic and the fundamental have a threshold at 75 W and the triiodide extinction threshold is 90 W. The different thresholds for luminescence and extinction are remarkable, since the activating chemical reaction has a similar starting point [5], which is the generation of hydroxide radicals.

The dependence of the indicators on the temperature for $U_S = 2.75$ V is shown in Fig. 8, normalised to their maximum value. The triiodide extinction was measured only up to 33 °C, the sound pressure up to 37 °C, because at high temperatures the transducers did not work sufficiently stable and the electrical power input had decreased.

All indicators show a maximum within the investigated temperature range (Fig. 6). Maximum values are reached first by erosion (15 °C), followed by luminescence (17 °C), rms pressure (20 °C), triiodide extinction (21 °C) and subharmonic (26 °C). For a detailed analysis that takes into account the variations in electrical power, see the second part of this paper [1].

Fig. 9 shows the dependence of the indicators on the O_2 concentration for $U_S = 2.75$ V and a temperature of 20 °C. Compared to the dependence on the electrical power (Fig. 7) and the temperature (Fig. 8), the indicators seem to be less affected. Luminescence is most sensitive to O_2 concentration changes. For very low O_2 concentration the luminescence is very high. In the range from 25% to 80% O_2 concentration, luminescence remains about constant and decreases for higher values. Thus, the normalizing factor for luminescence in this figure is about 10 times higher than in Fig. 7. The triiodide extinction is nearly constant but at a high level, compared to the former measurements. The scaling factor is four times higher than in the measurements shown before and the factor decreases as the O_2 concentration increases. This agrees with the measurements with gas-saturated water. In contrast to the

high levels of luminescence and triiodide extinction, the erosion is quite small and shows no systematic trend.

4. Discussion and outlook

In this paper, four sensor types were presented to determine indicators of cavitation. The sensing methods were chosen to serve as model processes which represent different aspects of cavitation effects. It could be shown that important process properties and conditions can be identified. For this purpose, the properties of the indicators and their relations to each other and to measurement parameters such as the dependence on the electrical input power, the temperature and the O_2 concentration of the water were investigated.

The properties of the water in the cleaning vessel were kept constant to be able to compare different measurement courses. For this purpose, a flow system was installed which continuously exchanged the water in the vessel. The flow was adjusted in such a way that the whole water volume of the vessel was exchanged within two minutes. So even in long measurement cycles, temperature variations could be limited to about 1 °C. O_2 saturated water did not degas significantly and degassed water only slowly accumulated air within a measurement course.

The four sensors are different in size and shape, and they influence the acoustic and the flow field in the vessel in different ways. The flow is most affected by the partially extended aluminium foil. The flow through the vessel is restricted to a small area near the bottom of the vessel and the local streams induced by the cavitation are restrained.

In contrast, the sound field is more strongly influenced by the sensors for sonochemistry and luminescence, especially if they are located near the transducer. In preceding experiments, instead of the test tubes, a thin-walled foil package was used. In fact, one can expect a smaller influence of these packages on the sound field because of the smaller wall thickness, and the size of the packages can be better adjusted to the experimental requirements. However, the shape of the packages varies; thus they can be positioned less

exactly and the sound absorbance varies with the shape of the surface. In addition, while filling these packages it is nearly impossible to prevent little air bubbles in the packages from forming and the foil often does not resist the strong cavitation field. Generally, by the absorption of the sound the isolated volumes heat up more than the surrounding water, where cavitation-induced streams exchange the water. This seriously effects the measurements, if the times of acoustic irradiation differ extremely. For large amplitudes and 4 min of irradiation for the sonochemical reaction the test tubes heated up significantly, whereas for the luminescence measurement irradiating the tubes for 15 s did not lead to any heating. The test tubes were a compromise between easy handling, influence on the sound field and stability of the experimental conditions for a localised measurement.

As preliminary tests, measurements were made with a hydrophone. It was investigated how measurements depend on the adjusted parameters using the different sensors. When changing the electrical power in a certain range, a hysteresis effect of the subharmonic was observed. This complicates the investigation of relations between the indicators because it is not clear when cavitation sets in. By using statistical analysis, the effects on the indicators caused by hysteresis and by spreading should be minimised.

Measurements with different sensors had to be performed subsequently, because in one measurement course only one sensor could be held at the measurement position and changing sensors takes a long time. To estimate the amount of uncertainty relating to two subsequent measurement cycles, the ultraharmonic and the subharmonic were investigated from two sequenced cycles. Comparing these indicators from different measurements with those from the same measurement, marginal differences in the behaviour of these indicators could be seen. The cavitation behaviour of succeeding measurements is thus quite similar. As mentioned before, it should be noted that the cavitation field is influenced by the sensors in different ways.

In one experiment, the subharmonic was measured at seven locations in the vessel. The water was O₂ saturated and the temperature was changed while the transducers were driven at several power settings. For all temperature settings, the subharmonic behaviour was unexpectedly uniform at the different positions. In nearly all cases the subharmonic threshold was independent of the measurement positions. In the shown measurement result significant spreading of data only occurred near 25 °C for $U_S = 2.5$ V and near 40 °C for $U_S = 1.75$ V.

Despite carefully controlling all measurement parameters and conditions, the results show a stochastic behaviour that is caused by the statistic nature of cavitation. So it seems to be appropriate to look for global trends by applying statistical methods, and in the accompanying paper, relations of the parameters and indicators were investigated using a factor analysis.

The scope of this study was restricted to a single cleaning vessel driven by a stable frequency. It would be interesting to see how the indicators behave if more parameters are changed, e.g. the frequency, the shape of the vessel or the surface tension by the addition of surfactants. It could be shown, however, that a determination of the four model indicators provides important and useful information about a cavitation process. This is considered to be a good basis for a general description of cavitation processes which can be applied to process optimization and process characterization, e.g. in a manufacturer's quality management system.

Acknowledgements

This work was supported by the DECHEMA, as a member of the AiF, in the program "Industrielle Gemeinschaftsforschung" (IGF). The authors thank Christoph Kling and Klaus-Vitold Jenderka for valuable discussions.

References

- [1] C. Koch, M. Jüschke, Model processes and cavitation indicators for a quantitative description of an ultrasonic cleaning vessel: Part II – Multivariate data analysis, *Ultrason. Sonochem.* 19 (2012) 796–802.
- [2] K.S. Suslick, Y. Didenko, M.M. Fang, T. Hyeon, K.J. Kolbeck, W.B. McNamara, M.M. Mdeleleni, M. Wong, Acoustic cavitation and its chemical consequences, *Philos. Trans. R. Soc. Lond. A* 357 (1999) 335–353.
- [3] T.J. Mason, J.P. Lorimer, *Applied Sonochemistry: Uses of Power Ultrasound in Chemistry and Processing*, Wiley, VCH, 2002.
- [4] D.L. Miller, Overview of experimental studies of biological effects of medical ultrasound caused by gas body activation and inertial cavitation, *Prog. Biophys. Mol. Biol.* 93 (2007) 314–330.
- [5] T.G. Leighton, *The Acoustic Bubble*, Academic Press, 1994.
- [6] U. Parlitz, R. Mettin, S. Luther, I. Akhatov, M. Voss, W. Lauterborn, Spatio-temporal dynamics of acoustic cavitation bubble clouds, *Philos. Trans. R. Soc. Lond. A* 357 (1999) 313–334.
- [7] W. Lauterborn, T. Kurz, Physics of bubble oscillations, *Rep. on Prog. Phys.* 73 (2010).
- [8] R. Mettin, S. Luther, C.D. Ohl, W. Lauterborn, Acoustic cavitation structures and simulations by a particle model, *Ultrason. Sonochem.* 6 (1999) 25–30.
- [9] D. Krefting, R. Mettin, W. Lauterborn, High-speed observation of acoustic cavitation erosion in multibubble systems, *Ultrason. Sonochem.* 11 (2004) 119–123.
- [10] M. Arora, C.D. Ohl, D. Lohse, Effect of nuclei concentration on cavitation cluster dynamics, *J. Acoust. Soc. Am.* 121 (2007) 3432–3436.
- [11] S. Kumar, C.E. Brennen, Nonlinear effects in the dynamics of clouds of bubbles, *J. Acoust. Soc. Am.* 89 (1991) 707–714.
- [12] W. Lauterborn, T. Kurz, R. Mettin, C.D. Ohl, Experimental and theoretical bubble dynamics, *Adv. Chem. Phys.* 110 (1999) 295–380.
- [13] ANSI Technical Report, Bubble Detection and Cavitation Monitoring, ANSI S1.24 TR-2002, 2002.
- [14] B.N. Poddubnyi, Improvement of erosion-test methods based on aluminium foil damage and on sample weight loss, *Sov. Phys. Acoust.* 22 (1976) 325–327.
- [15] C. Wu, N. Nakagawa, M. Fujihara, Study on Acoustic Cavitations in the Ultrasonic Radiation Field, *JSME Int. J. Ser. C* 49 (2006) 758–763.
- [16] T.G. Leighton, A Strategy for the Development and Standardisation of Measurement Methods for High Power/Cavitating Ultrasonic Fields: Review of Cavitation Monitoring Techniques, Tech. Rep., Inst. Sound Vib. Res, Univ. Southampton, 1997.
- [17] B. Avvaru, A.B. Pandit, Experimental investigation of cavitation bubble dynamics under multi-frequency system, *Ultrason. Sonochem.* 15 (2008) 578–589.
- [18] B. Pugin, Qualitative characterization of ultrasound reactors for heterogeneous sonochemistry, *Ultrasonics* 25 (1987) 49–55.
- [19] V. Moholkar, S. Sable, A. Pandit, Mapping the cavitation intensity in an ultrasonic bath using the acoustic emission, *AIChE J.* 46 (2000) 684–694.
- [20] K.V. Jenderka, C. Koch, Investigation of spatial distribution of sound field parameters in ultrasound cleaning baths under the influence of cavitation, *Ultrasonics* 44 (2006) 401–406.
- [21] G. Vereecke, E. Parton, F. Holsteys, K. Xu, R. Vos, P.W. Mertens, M.O. Schmidt, T. Bauer, Investigating the role of gas cavitation in megasonic nanoparticle removal, *Micro* 22 (2004) 57–63.
- [22] E.A. Neppiras, Measurement of acoustic cavitation, *IEEE Trans. Son. Ultrason.* 15 (1968) 81–88.
- [23] N. Segebarth, O. Enlaerts, J. Reisse, L.A. Crum, T.J. Matula, Correlation between acoustic cavitation noise, bubble population, and sonochemistry, *J. Phys. Chem. B* 106 (2002) 9181–9190.
- [24] P. Gogate, P. Tatak, P. Kanthale, A. Pandit, Mapping of sonochemical reactors: review, analysis and experimental verification, *AIChE J.* 48 (2002) 1542–1560.
- [25] L. Hallez, F. Touyeras, J. Hihn, J. Klima, Energetic balance in an ultrasonic reactor using focused or flat high frequency transducers, *Ultrason. Sonochem.* 14 (2007) 739–749.
- [26] Y. Son, M. Lim, J. Khim, M. Ashokkumar, Acoustic emission spectra and sonochemical activity in a 36 kHz sonoreactor, *Ultrason. Sonochem.* 19 (2012) 16–21.
- [27] D.M. Hallow, A.D. Mahajan, T.E. McCutchen, M.R. Prausnitz, Measurement and correlation of acoustic cavitation with cellular bioeffects, *Ultrasound Med Biol.* 32 (2006) 1111–1122.
- [28] T.D. Mast, V.A. Salgaonkar, C. Karunakaran, J.A. Bessea, S. Dattaa, C.K. Hollanda, Acoustic emissions during 3.1 MHz ultrasound bulk ablation in vitro, *Ultrasound Med Biol.* 34 (2008) 1434–1448.
- [29] C. Kling, C. Koch, K.V. Jenderka, Space-resolved sonochemistry in cleaning vessels in comparison to mechanical effects, International Conference on Acoustics, Rotterdam (2009) 1354–1356.
- [30] A. Weissler, H.W. Cooper, S. Snyder, Chemical effect of ultrasonic waves: oxidation of potassium iodide solution by carbon tetrachloride, *J. Am. Chem. Soc.* 72 (1950) 1769–1775.
- [31] K. Negishi, Experimental Studies on Sonoluminescence and Ultrasonic Cavitation, *J. Physical Soc. Japan.* 16 (1961) 1450–1465.
- [32] A. Henglein, R. Ulrich, J. Lillie, Luminescence and chemical action by pulsed ultrasound, *J. Am. Chem. Soc.* 111 (1989) 1974–1979.